A nonlinear weakly dispersive method for recovering the elevation of irrotational surface waves from pressure measurements

P. Bonneton [a,*], D. Lannes [b], K. Martins [c], H. Michallet [d]

[a] *University of Bordeaux, CNRS, UMR 5805 EPOC, Allée Geoffroy Saint-Hilaire, F-33615 Pessac, France*
[b] *University of Bordeaux, IMB and CNRS UMR 5251, Talence, F-33405, France*
[c] *UMR 7266 LIENSs, CNRS-Université de La Rochelle, 2 rue Olympe de Gouges, La Rochelle, 17000, France*
[d] *University Grenoble Alpes, CNRS, LEGI, CS40700, 38058 Grenoble, France*

ARTICLE INFO

ABSTRACT

We present the derivation of a nonlinear weakly dispersive formula to reconstruct, from pressure measurements, the surface elevation of nonlinear waves propagating in shallow water. The formula is simple and easy to use as it is local in time and only involves first and second order time derivatives of the measured pressure. This novel approach is evaluated on laboratory and field data of shoaling waves near the breaking point. Unlike linear methods, the nonlinear formula is able to reproduce at the individual wave scale the peaked and skewed shape of nonlinear waves close to the breaking point. Improvements in the frequency domain are also observed as the new method is able to accurately predict surface wave elevation spectra over four harmonics. The nonlinear weakly dispersive formula derived in this paper represents an economic and easy to use alternative to direct wave elevation measurement methods (e.g. acoustic surface tracking and LiDAR scanning).

1. Introduction

Near-bottom-mounted pressure sensors have long been used for measuring surface wave in the nearshore. However, the relationship between bottom pressure and sea surface elevation is not straightforward. This relationship is commonly assumed to be given by linear wave theory, the so-called transfer function method (e.g. Bishop and Donelan (1987) and Tsai et al. (2005)). The validity of this linear reconstruction has been extensively studied in field conditions for waves propagating in relatively shallow water (Hom-ma et al., 1966; Esteva and Harris, 1970; Cavaleri et al., 1978; Guza and Thornton, 1980). Although discrepancies were greater close to the break point, Guza and Thornton (1980) found a good agreement in and outside the surf zone between sea surface elevation spectra derived from pressure data and from direct elevation measurements. Errors in both total variance and energy density in a particular frequency band were less than 20%. In a more controlled environment, Bishop and Donelan (1987) estimated that using linear wave theory was leading to error of about 5% of the wave height; uncertainty in the deployment of *in situ* instruments and the data itself was thought to be responsible for the varying error estimates found in the literature. Following these seminal studies, the linear reconstruction method has become the main approach for characterizing shallow-water surface-wave elevation in field conditions.

This approach is commonly used for determining bulk wave parameters such as the significant wave height H_s, but it has also served as a basis for studying nonlinear wave interactions in the field (e.g. Elgar and Guza (1985), Elgar et al. (1997), Senechal et al. (2002), Henderson et al. (2006)). However, we know that wave nonlinearities can be strong in the shoaling zone, especially in the region close to the onset of breaking, and thus the use of a linear theory to reconstruct wave elevation can be questioned. For instance, Bonneton and Lannes (2017) and Martins et al. (2017a) have shown that the linear reconstruction fails to describe the peaky and skewed shape of nonlinear waves, and lead to an underestimation of the individual wave height by up to 30% just prior the breaking point (Martins et al., 2017a). Such measurement errors are problematic for many coastal applications, such as studies on wave overtopping and submersion which require accurate measurements of the highest wave crests. Furthermore, a correct description of wave asymmetry and skewness is of paramount importance for understanding sediment dynamics (e.g. Dubarbier et al. (2015)). Finally, an accurate description of the wave elevation field is also crucial for the validation of the new generation of fully-nonlinear phase-resolving wave models (e.g. Zijlema et al. (2011), Bonneton et al. (2011) or Shi et al. (2012)).
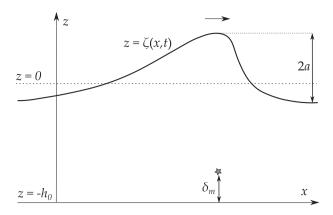
Even if some methods are now available for a direct measurement of

---

Fig. 1. Sketch of the Cartesian coordinate system: x is the horizontal axis along which waves propagate and z points vertically upwards, with $z = 0$ being the mean water level and $z = -h_0$ the distance to the bottom. The wave amplitude is noted a and δ_m represents the distance to the bottom at which the pressure is measured.

the surface elevation, such as acoustic surface tracking (Birch et al., 2004) or LiDAR scanning (Martins et al., 2016), pressures sensors remain a very useful tool for coastal wave applications. Indeed, they are cheap, robust, not sensitive to air bubbles or turbidity, and easy to deploy since they do not require the presence of nearshore infrastructure, as it can be the case for LiDAR technology [e.g., see (Martins et al., 2017c)]. Bonneton and Lannes (2017) recently derived a method which allows a fully dispersive nonlinear reconstruction of the surface elevation from pressure measurements. Comparisons with numerical Euler solutions and laboratory data showed that this nonlinear method provides much better results than the classical linear approach. It gives an accurate prediction of the maximum elevation and, contrary to the nonlinear heuristic method proposed by Oliveras et al. (2012), it accurately reproduces the skewed shape of nonlinear dispersive wave fields. However, this method requires, like the classical linear transfer approach (Bishop and Donelan, 1987; Tsai et al., 2005) and the heuristic method (Oliveras et al., 2012; Vasan et al., 2017), the use of a frequency cutoff which becomes a limiting factor for the reconstruction of strongly nonlinear waves. In the present paper we derive a nonlinear weakly-dispersive method which allows an accurate reconstruction of nonlinear waves in shallow water, especially just prior to breaking.

2. Nonlinear weakly-dispersive reconstruction formula

In this section we derive a formula working in the time domain, which allows the elevation reconstruction of nonlinear shallow water waves from pressure measurements. This formula is an approximate expression, in the shallow water regime, of the fully dispersive formula derived in (Bonneton and Lannes, 2017). The derivation presented in this section is much simpler and straightforward compared to the general fully dispersive derivation.

We consider that the wave field is locally close to a two-dimensional wave field. We choose Cartesian coordinates (x, z), where x is the horizontal axis along which waves propagate and z the upward vertical coordinate. We denote $z = \zeta(x, t)$ the elevation of the free surface above the still water level $z = 0$, and by $z = -h_0$ the constant bottom elevation (see Fig. 1). The water depth h can be expressed as $h(x, t) = h_0 + \zeta(x, t)$. The pressure P_m is measured at a distance δ_m above the bottom, $P_m = P|_{z=-h_0+\delta_m}$, where $P(x, z, t)$ is the pressure field.

The fluid motion is governed by the free-surface incompressible irrotational Euler equations; if the flow is irrotational, as it is assumed here, it is convenient to work with a velocity potential instead of the velocity field, and with Bernoulli's equation instead of Euler equations. If ϕ denotes the velocity potential, these equations can be recast in the form:

$$\partial_x^2 \phi + \partial_z^2 \phi = 0$$

$$\partial_t \phi + gz + \frac{1}{2}|\partial_x \phi|^2 + \frac{1}{2}|\partial_z \phi|^2 = -\frac{1}{\rho}(P - P_{atm}),$$

where ρ is the water density, g the gravity and P_{atm} the (constant) atmospheric pressure. These equations are complemented by boundary conditions. At the bottom we have

$$\partial_z \phi = 0 \quad \text{on } z = -h_0; \tag{1}$$

at the surface, we have the classical kinematic equation on ζ,

$$\partial_t \zeta = \partial_z \phi - \partial_x \zeta \cdot \partial_x \phi \quad \text{on} \quad z = \zeta, \tag{2}$$

and the pressure continuity,

$$P = P_{atm} \quad \text{on} \quad z = \zeta. \tag{3}$$

Three main length scales are involved in this problem: the characteristic horizontal length L ($L = 1/k$, where k is the typical wave number), the amplitude a of the wave, and the depth at rest h_0. The problem is then controlled by two dimensionless parameters:

$$\varepsilon = \frac{a}{h_0}, \qquad \mu = \frac{h_0^2}{L^2} = (h_0 k)^2$$

where ε is a nonlinearity parameter while μ is the shallowness parameter. The different variables and functions involved in this problem can be put in dimensionless form using the relations

$$x' = \frac{x}{L}, \quad z' = \frac{z}{h_0}, \quad \delta'_m = \frac{\delta_m}{h_0}, \quad t' = \frac{\sqrt{gh_0}}{L}t,$$

$$\zeta' = \frac{\zeta}{a}, \quad h' = \frac{h}{h_0} = 1 + \varepsilon\zeta', \quad \phi' = \frac{h_0}{aL\sqrt{gh_0}}\phi, \quad P' = \frac{P}{\rho gh_0},$$

where the primes are used to denote dimensionless quantities. Omitting the primes for the sake of clarity, the vertical momentum equation, in dimensionless form, writes

$$\varepsilon\Gamma = -1 - \partial_z P,$$

where $\Gamma = \partial_t w + \varepsilon u\partial_x w + \frac{\varepsilon}{\mu}w\partial_z w$ is the vertical acceleration, $u = \partial_x \phi$ the horizontal velocity and $w = \partial_z \phi$ the vertical velocity. Integrating this equation over z we get

$$\zeta = \zeta_H - \int_{-1+\delta_m}^{\varepsilon\zeta} \Gamma dz \tag{4}$$

where ζ_H is the dimensionless hydrostatic reconstruction

$$\zeta_H = \frac{1}{\varepsilon}(P_m - P_{atm} - 1 + \delta_m). \tag{5}$$

The Formula (4) is exact but involves quantities that cannot be expressed in terms of the measured pressure P_m. Our goal is to derive approximate formulas that can be expressed as a function of P_m, or equivalently ζ_H. Following (Lannes and Bonneton, 2009), we shall perform an asymptotic expansion of (4) in terms of the shallowness parameter μ.

The velocity potential ϕ is given at second order by

$$\phi = \psi - \frac{\mu}{2}\left((z+1)^2 - h^2\right)\partial_x^2 \psi + O(\mu^2), \tag{6}$$

with $\psi = \phi|_{z=\varepsilon\zeta}$. From this equation we can deduce that

$$u = U + O(\mu)$$

$$w = -\mu(z+1)\partial_x U + O(\mu^2),$$

where U is the depth-averaged horizontal velocity. Using these relations Eq. (4) becomes

$$\zeta = \zeta_H - \frac{\mu}{2}\left(h^2 - \delta_m^2\right)\left(\partial_x^2\zeta + 2\varepsilon(\partial_x U)^2\right) + O(\mu^2). \tag{7}$$

From the linearized water waves equations in shallow water, we know that $\partial_t^2\zeta - \partial_x^2\zeta = O(\varepsilon, \mu)$, and the above formula therefore yields

$$\partial_x^2\zeta_H = \partial_t^2\zeta_H + O(\varepsilon, \mu). \tag{8}$$

For weakly nonlinear waves ($\varepsilon = O(\mu)$) we deduce a linear shallow water reconstruction formula from (7) and (8),

$$\zeta_{SL} = \zeta_H - \frac{\mu}{2}\left(1 - \delta_m^2\right)\partial_t^2\zeta_H, \tag{9}$$

which is valid up to terms of order $O(\varepsilon\mu, \mu^2)$.

For moderately nonlinear waves ($\varepsilon = O(\mu^{1/2})$) the $O(\varepsilon\mu)$ terms cannot be neglected, and we therefore seek a higher order correction of (9) under the form

$$\zeta_{SNL} = \zeta_{SL} + \varepsilon\mu C,$$

where the corrector term C is chosen in such a way that Eq. (7) is satisfied up to $O(\mu^2)$ terms if ζ is replaced by ζ_{SNL}. This yields the condition

$$-\frac{\mu}{2}\left(1 - \delta_m^2\right)\left(\partial_t^2\zeta_H - \partial_x^2\zeta_H\right) + \varepsilon\mu C = -\varepsilon\mu\left(\zeta\partial_x^2\zeta + \left(1 - \delta_m^2\right)(\partial_x U)^2\right) + O(\mu^2)$$

From the mass conservation equation $\partial_t\zeta + \partial_x(hU) = 0$, we deduce that $\partial_x U = -\partial_t\zeta + O(\varepsilon)$ which, together with (8) yields

$$\partial_t^2\zeta_H - \partial_x^2\zeta_H = \frac{2\varepsilon}{1 - \delta_m^2}\left(C + \partial_t(\zeta\partial_t\zeta) - \delta_m^2(\partial_t\zeta)^2\right) + O(\mu).$$

The $O(\varepsilon)$ terms gathers the quadratic interactions of the wave field. Since at order $O(\varepsilon, \mu)$, the waves are governed by a linear wave equation with speed 1, these quadratic terms are either the product of co-propagating or counter-propagating waves and therefore of the form

$$\partial_t^2\zeta_H - \partial_x^2\zeta_H = \varepsilon(F(x - t) + G(x + t) + \mathscr{F}(x - t)\mathscr{G}(x + t)) + O(\mu),$$

for some functions F and G that depend quadratically on ζ and some functions $\mathscr{F}$ and $\mathscr{G}$ that depend linearly on ζ.

The only possibility that does not create secular growth for ζ_H is if the right-hand-side is equal to zero (see for instance (Lannes, 2003) or Lemma 7.20 in (Lannes, 2013)). This corresponds to

$$C = -\partial_t(\zeta\partial_t\zeta) + \delta_m^2(\partial_t\zeta)^2.$$

Since $\zeta = \zeta_{SL} + O(\mu)$, we therefore obtain the following nonlinear shallow water reconstruction formula

$$\zeta_{SNL} = \zeta_{SL} - \varepsilon\mu\left(\partial_t(\zeta_{SL}\partial_t\zeta_{SL}) - \delta_m^2(\partial_t\zeta_{SL})^2\right), \tag{10}$$

which is valid up to $O(\mu^2)$ terms for moderately nonlinear waves. A generalization of this formula in presence of a background current is given in (Bonneton and Lannes, 2017).

The reconstruction formula (10) has been derived under the assumption of a locally flat bottom. We can easily extend this approach by taking into account a slowly varying bathymetry. The bottom is given by $z = -h_0 + b(x)$, where b is a slowly varying function of x. The nonlinear reconstruction becomes in dimensionless form

$$\zeta = \zeta_{SNL} + \sqrt{\mu}\sigma_b\partial_x b\partial_x\zeta + O(\mu^2, \mu\sigma_b),$$

where σ_b is the characteristic slope of the bathymetry at the measurement location. For unidirectional traveling waves the nonlinear reconstruction simplifies to the form which follows

$$\zeta = \zeta_{SNL} - \sqrt{\mu}\sigma_b\partial_x b\partial_t\zeta_{SNL} + O(\mu^2, \mu\sigma_b).$$

The parameter $\sqrt{\mu}\sigma_b$ being very small for many coastal applications, as those discussed in section 3, we neglect throughout the paper the bottom contribution.

In variables with dimension the reconstruction formulas (5), (9) and (10) become

$$\zeta_H = \frac{P_m - P_{atm}}{\rho g} - h_0 + \delta_m \tag{11}$$

$$\zeta_{SL} = \zeta_H - \frac{h_0}{2g}\left(1 - (\delta_m/h_0)^2\right)\partial_t^2\zeta_H \tag{12}$$

$$\zeta_{SNL} = \zeta_{SL} - \frac{1}{g}\left(\partial_t(\zeta_{SL}\partial_t\zeta_{SL}) - (\delta_m/h_0)^2(\partial_t\zeta_{SL})^2\right). \tag{13}$$

Contrary to fully dispersive reconstructions (see (Bonneton and Lannes, 2017)) these formulas can be applied locally in time and do not necessarily require Fourier transforms (see Appendix A). The ability of these formulas to reconstruct shallow water waves was first assessed by (Bonneton and Lannes, 2017) from comparison with solitary wave solutions computed from the Euler equations. In the next section the validation is extended to nonlinear shallow water waves propagating on gently sloping bottoms.
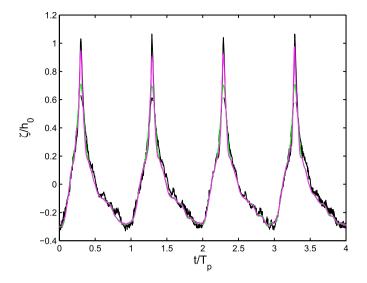
3. Applications to laboratory and field data

To assess the ability of the formulas derived in the preceding section we use laboratory and field data corresponding to weakly dispersive waves ($\mu \leq 0.28$) propagating in the shoaling zone close to the breaking point. Such test cases, which are associated with strong nonlinearities (i.e. large ε), represent highly demanding cases for surface wave reconstruction.

The reconstructed elevation is obtained from pressure signals measured under waves and then compared to direct elevation measurements. The application of formulas (12) and (13) requires to compute first and second order time derivatives of the measured pressure P_m, or equivalently ζ_H. To compute these derivatives, it is recommended to filter the measurement noise, either using a local filter (e.g. moving average filter) or a spectral filter. In the present study we use a low-pass spectral filter with a cut-off frequency f_c. Linear and nonlinear fully dispersive reconstructions (e.g. (Bishop and Donelan, 1987; Guza and Thornton, 1980; Bonneton and Lannes, 2017; Vasan et al., 2017)) also require introducing a cut-off frequency. However, it is worth noting that this fully-dispersive cut-off is much more restrictive (i.e. much lower f_c used) than that required for the present weakly dispersive reconstructions. Indeed, the frequency cut-off used in fully dispersive reconstructions is not fixed by the level of noise in the measurements but by the level of wave nonlinearity and the error originating from the use of the linear dispersion relation for the estimation of the nonhydrostatic correction factor $\cosh(kh_0)$.
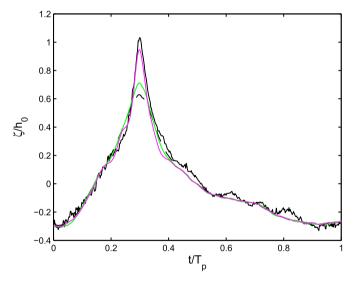
In order to accurately compute the time derivatives involved in equations (12) and (13) we have chosen to use a Fourier transform method. The use of a local time discretization approach for solving the time derivatives is also discussed in appendix A. For the shallow water applications presented in this paper, the shallow water linear reconstruction (12) gives performance at least as good as those given by the fully dispersive linear reconstruction (the classical so-called transfer function formula, see (Bishop and Donelan, 1987)). For that reason, we do not present linear transfer function reconstruction in the following validations.

3.1. Monochromatic waves

We first use experimental data from the A7-mono test obtained during the BARDEXII set of experiments (Masselink et al., 2016), performed at

Fig. 2. Surface elevation reconstruction of monochromatic waves. A7-mono test obtained during BARDEXII, $h_0 = 1.17$ m, $T_p = 12.1$ s and $\delta_m = 0.33$ m. Dimensionless cut-off frequency $T_p f_c = 20$. black line: direct LiDAR measurement of ζ; dashed black line: hydrostatic reconstruction ζ_H, Eq. (11); green line: ζ_{SL}, Eq. (12); magenta line: ζ_{SNL}, Eq. (13). (For interpretation of the references to colour in this figure legend, the reader is referred to the Web version of this article.)

Fig. 3. Surface elevation reconstruction of monochromatic waves. Zoom over one period of A7-mono test obtained during BARDEXII, $h_0 = 1.17$ m, $T_p = 12.1$ s and $\delta_m = 0.33$ m. Dimensionless cut-off frequency $T_p f_c = 20$. black line: direct LiDAR measurement of ζ; dashed black line: hydrostatic reconstruction ζ_H, Eq. (11); green line: ζ_{SL}, Eq. (12); magenta line: ζ_{SNL}, Eq. (13). (For interpretation of the references to colour in this figure legend, the reader is referred to the Web version of this article.)

prototype-scale in the Delta flume, Vollenhove, The Netherlands. Martins et al. (2017a) used pressure and surface elevation data obtained from a LiDAR scanner from this test to validate the simulated wave transformation across the wave flume. Although the datasets are described in Martins et al. (2017a), some basic information are reminded here.

Second-order monochromatic Stokes waves ($T = 12.1$s, $H = 0.68$m) were generated in the experimental flume. The pressure was measured just before the break point, with a sampling frequency of 20 Hz. The pressure sensor was situated at a distance $\delta_m = 0.33$m above the bottom. For this wave test, the still water depth was $h_0 = 1.17$m, the characteristic bottom slope was $\sigma_b = 0.041$ and the values of the dimensionless

Table 1
Sea surface skewness. Comparison between reconstructed elevation and direct LiDAR elevation measurements.

	ζ_H, eq. (11)	ζ_{SL}, eq. (12)	ζ_{SNL}, eq. (13)	ζ_{LiDAR}
S_k	0.98	1.12	1.46	1.45
S_k error	32.2 %	22.5 %	0.7 %	–

parameters were $\mu = 0.032$ and $\varepsilon = 0.65$. It is worth noting that the pressure data was obtained close to the breaking point (Martins et al., 2017a), where nonlinearities are the strongest and close to a crest anti-node, due to the strong reflection experienced during the test.

The LiDAR scanner consisted of a LMS511 SiCK eye-safe ($\lambda = 905$ nm) 2D scanner deployed 3.9 m above the still water level, a meter landward of the pressure transducer. Unlike the pressure transducer, the scanner directly detects the surface by capturing back the light beam scattered at the surface by the presence of ripples/roughness or air bubbles in case of breaking. The LiDAR data were collected at 37.5 Hz, and only the data at the pressure transducer location is used. For this specific experiment the LiDAR measurement accuracy was about 0.02 m. The reader is referred to Martins et al., 2016, 2017a for more details on the scanner data processing.

Fig. 2 presents a comparison, over four wave periods, between reconstructed wave elevation and direct LiDAR measurements. We can see that in this shallow water regime the linear reconstruction (12) brings little improvement in comparison with the hydrostatic formula (11) and strongly underestimates the crest elevation. A wave by wave analysis shows that the root mean square (RMS) error for the wave height estimated from the linear reconstruction reaches 28% (see also (Martins et al., 2017a)). By contrast, the nonlinear formula (13) gives much better results. In particular, we can see in Fig. 3 that the peaked and skewed shape of the wave is much better described by the nonlinear formulation Eq. (13) than by the linear one Eq. (12). In order to quantify the wave asymmetry with respect to the horizontal axis we have computed the skewness parameter:
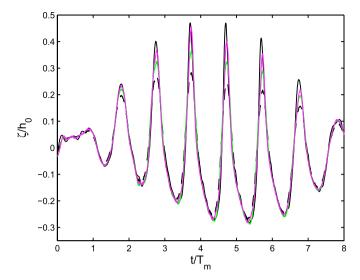
$$S_k = \frac{\langle (\zeta - \langle \zeta \rangle)^3 \rangle}{\langle (\zeta - \langle \zeta \rangle)^2 \rangle^{3/2}},$$

where $\langle . \rangle$ is the time-averaging operator. Table 1 shows that the linear reconstruction strongly underestimates, by 22.5%, the wave skewness. By contrast the skewness is very well reproduced by the nonlinear reconstruction with an error, for this specific test case, smaller than 1%. The nonlinear formula also improves the evaluation of the wave crest elevation (RMS error of 17%), but less significantly compared with the skewness.
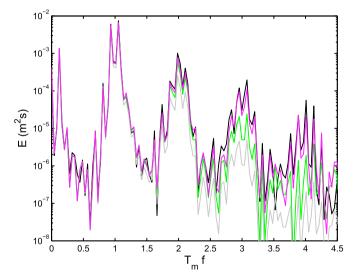
The skewness parameter is related to the velocity skewness at the bed (see e.g. Rocha et al. (2017)) which, along with the wave asymmetry, can be used to compute the sediment transport rate (e.g. Abreu et al. (2013)). The wave high order harmonics also contribute to the acceleration effects that can promote bed motion (e.g. Berni et al. (2017)). This underlines the need to accurately characterize wave non-linearities for predicting sediment transport and morphodynamics (e.g. Dubarbier et al. (2015)).

3.2. Bichromatic waves

In this section, the ability of our shallow water formulas to reconstruct nonlinear waves is assessed with respect to a bichromatic wave field propagating over a gently sloping (1/20) movable bed. The small-scale experimental set-up is described in Michallet et al. (2017) and references therein. The two frequencies composing the wave-board motion were $f_1 = 0.5515$ Hz and $f_2 = 0.6250$ Hz, and the amplitude of the two wave components were identical with a value of 0.03 m. Water elevation and bottom pressure were synchronously measured (at 128 Hz) in the shoaling zone, just prior to wave breaking. The surface elevation was monitored with a capacitive wave gauge. Its accuracy was estimated
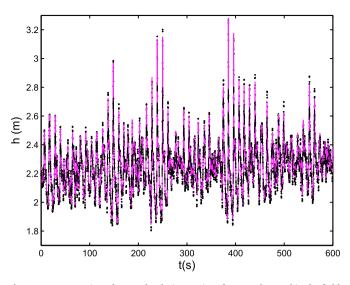
Fig. 4. Surface elevation reconstruction of bichromatic waves, $f_1 = 0.5515$ Hz, $f_2 = 0.6250$ Hz $\left(T_m = \left(\frac{f_1+f_2}{2}\right)^{-1}\right)$, $h_0 = 0.185$ m and $\delta_m = 0$. Dimensionless cut-off frequency $T_m f_c = 4.5$. black line: direct measurement of ζ; dashed black line: hydrostatic reconstruction ζ_H, Eq. (11); green line: ζ_{SL}, Eq. (12); magenta line: ζ_{SNL}, Eq. (13). (For interpretation of the references to colour in this figure legend, the reader is referred to the Web version of this article.)

Fig. 5. Surface elevation energy density spectra, $E(f)$, as a function of the dimensionless frequency $T_m f$, for bichromatic waves, $f_1 = 0.5515$ Hz, $f_2 = 0.6250$ Hz $\left(T_m = \left(\frac{f_1+f_2}{2}\right)^{-1}\right)$, $h_0 = 0.185$ m and $\delta_m = 0$. Dimensionless cut-off frequency $T_m f_c = 4.5$. black line: direct measurement of ζ; grey line: hydrostatic reconstruction ζ_H, Eq. (11); green line: ζ_{SL}, Eq. (12); magenta line: ζ_{SNL}, Eq. (13). (For interpretation of the references to colour in this figure legend, the reader is referred to the Web version of this article.)
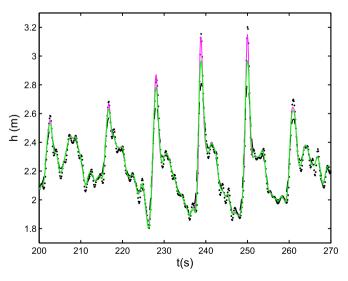
to be of approximately 1 mm from comparison with high-speed video recordings. The pressure sensor was located at the bed. The still water depth at the measurement location was $h_0 = 0.185$ m, the characteristic bottom slope was $\sigma_b = 0.08$ and the values of the dimensionless parameters were $\mu = 0.28$ and, for the highest wave of the group, $\varepsilon = 0.37$.

Fig. 4 presents a comparison between shallow water reconstructions and direct elevation measurements. The nonlinear formula (13) significantly improves the elevation reconstruction compared with the linear formula (12), especially for the highest waves. The prediction is slightly
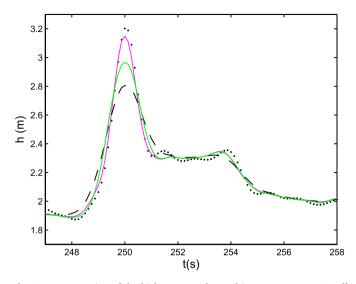

Fig. 6. Reconstruction of water depth time series of waves observed in the field. Cut-off frequency $f_c = 1$ Hz, $\overline{h} = 2.25$ m, $\delta_m = 0.69$ m. dot: direct acoustic measurement of h; magenta line: $h_{SNL} = \overline{h} + \zeta_{SNL}$, Eq. (13).
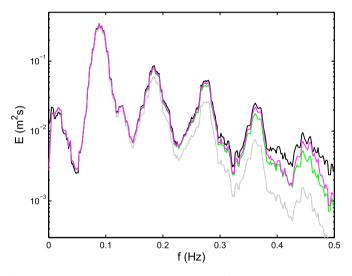
poorer at the wave crests in the second half of the wave packet. It was observed that the erosion depth and the mobile sediment layer thickness were enhanced after the highest wave. Further investigations would be needed to confirm how the sediment dynamics might contribute to damp high frequencies at the sensor location. Fig. 5 shows a comparison between the measured surface elevation energy density spectrum and the spectra obtained from reconstruction formulas. We can see that the linear (12) and nonlinear (13) reconstructions properly describe the elevation energy around the first (i.e. fundamental) harmonic. For higher harmonics, the agreement between the linear reconstruction (12) and direct measurements significantly decreases. Fig. 5 shows that the linear theory underestimates the energy around the 4th harmonic by more than one order of magnitude. By contrast, our nonlinear formula (13) accurately predicts the wave spectrum over the four harmonics. This result demonstrates that a nonlinear approach is essential for nonlinear wave reconstruction.

Fig. 7. Reconstruction of water depth time series of a group of waves observed in the field. Cut-off frequency $f_c = 1$ Hz, $\overline{h} = 2.25$ m, $\delta_m = 0.69$ m. dot: direct acoustic measurement of h; green line: $h_{SL} = \overline{h} + \zeta_{SL}$, Eq. (12); magenta line: $h_{SNL} = \overline{h} + \zeta_{SNL}$, Eq. (13). (For interpretation of the references to colour in this figure legend, the reader is referred to the Web version of this article.)

Fig. 8. Reconstruction of the highest wave observed in a wave group. Cut-off frequency $f_c = 1$ Hz, $\bar{h} = 2.25\,m$, $\delta_m = 0.69$ m. dot: direct acoustic measurement of h; dashed black line: hydrostatic reconstruction ζ_{H}, Eq. (11); green line: $h_{\mathrm{SL}} = \bar{h} + \zeta_{\mathrm{SL}}$, Eq. (12); magenta line: $h_{\mathrm{SNL}} = \bar{h} + \zeta_{\mathrm{SNL}}$, Eq. (13). (For interpretation of the references to colour in this figure legend, the reader is referred to the Web version of this article.)

Fig. 9. Surface elevation energy density spectra, $E(f)$, of waves observed in the field. The spectra have been smoothed with a moving average over a window of $1/60$ Hz black line: direct measurement of ζ; grey line: hydrostatic reconstruction ζ_{H}, Eq. (11); green line: ζ_{SL}, Eq. (12); magenta line: ζ_{SNL}, Eq. (13). (For interpretation of the references to colour in this figure legend, the reader is referred to the Web version of this article.)

3.3. Field data

The data was collected during a field campaign performed on April 13–14 2017, at La Salie beach, situated on the southern part of the French Atlantic coast. Several instruments were deployed at low tide to characterize the shallow water wave field: a stereophotogrammetry system, a Nortek Signature 1000 kHz current profiler, a Nortek Aquadopp current meter and pressure transducers (Ocean Sensor Systems). At the deployment location the characteristic bottom slope was $\sigma_b = 0.015$. In the present paper we focus only on one 10-min data set (see Fig. 6) corresponding to nonlinear shallow water waves. Together with bottom pressure measurements (10 Hz sampling rate), a direct measurement of the surface elevation was obtained from the vertical beam of the

Signature 1000 kHz (8 Hz sampling rate). The video recording shows that the highest waves were breaking just shoreward of the sensors. Martins et al. (2017b) recently compared surface elevation measurements from LiDAR and a Signature 1000 kHz in the Garonne River during a non-breaking undular tidal bore event. Despite the high-turbidity environment, the acoustic sensor performed extremely well in tracking the free surface and estimating individual wave heights (*RMS* error of 0.05 m).

The wave conditions at the water depth $\bar{h} = 2.25$ m were characterized by a significant wave height of 0.70 m, with a peak period of 11.1 s ($\mu = 0.075$); large-amplitude wave groups were also observed (see Fig. 6). The maximum wave height in these wave groups is 1.4 m, which corresponds to a nonlinearity parameter ε of 0.31. Fig. 7 shows that the linear reconstruction (12) gives good results for the lowest waves of the wave group but strongly underestimates the elevation at the crest of the highest waves. On the other hand, our nonlinear formula (13) gives excellent results even for the highest waves. A zoom around the highest wave of the wave group observed in Fig. 7 is presented in Fig. 8. We can see in this figure that the linear reconstruction fails to predict the maximum elevation and above all the skewed shape of this nonlinear wave. By contrast, these wave properties are very well reproduced by the nonlinear reconstruction (13). The measured surface elevation energy density spectrum and the spectra obtained from reconstruction formulas are compared in Fig. 9. In agreement with observations for laboratory bichromatic waves (see Fig. 5) we can see that a nonlinear method is required to properly reconstruct the surface elevation spectrum, especially for the highest harmonics.

4. Conclusion

We have derived a nonlinear weakly dispersive formula (Eq. (13)) to reconstruct, from pressure measurements, the surface elevation of nonlinear waves propagating in shallow water. This simple and easy to use formula is local in time, only involving first and second order time derivatives of the measured pressure P_{m}, or equivalently ζ_{H}. Contrary to fully dispersive reconstruction formulas it does not necessarily require Fourier transform. The ability of this formula to reconstruct surface elevation has been assessed from laboratory and field experiments of weakly dispersive waves ($\mu \leq 0.28$) propagating in the shoaling zone just prior to breaking. Despite the strong nonlinearities naturally found close to the breaking point, and even in the presence of strong wave reflection (Section 3.1), the novel method was found to perform very well.

We have shown that the nonlinear formula (13) provides much better reconstructed surface elevation than linear methods. Our nonlinear reconstruction is able to accurately reproduce the peaked and skewed shape of nonlinear waves prior to breaking. Although the linear reconstruction method properly describes the surface elevation energy density around the fundamental harmonic, it strongly underestimates the energy density for the higher harmonics. In contrast, the nonlinear weakly dispersive reconstruction (13) accurately predicts the surface wave elevation spectrum over four harmonics. This demonstrates that a nonlinear approach is essential for nonlinear wave reconstruction in the shoaling zone and especially near the breaking point. However, the derivation of our nonlinear formula (Eq. (13)) is based on a shallowness assumption. For nonlinear waves propagating in intermediate water depth a fully dispersive nonlinear reconstruction is required (see Bonneton and Lannes (2017)).

An accurate description of surface wave elevation is crucial for many coastal applications, such as wave-induced sediment transport or overtopping and submersion associated with extreme waves. In this context, the application of nonlinear reconstruction methods on pressure data represent an economic and easy to use alternative to direct wave elevation measurement methods, such as acoustic surface tracking or LiDAR scanning that can be hard to deploy in some circumstances.

Acknowledgments

Appendix A. Local time discretization method for the surface reconstruction

In contrast to fully dispersive reconstructions, the weakly dispersive methods derived in the present paper are local in time and thus do not necessarily require the use of Fourier transforms. However, to accurately compute time derivatives and to easily filter out the measurement noise we have used Fourier transforms in this paper (see section 3). When the measured pressure time series is too short for a Fourier analysis a local time discretization method is required. The time derivatives involved in equations (12) and (13) can be computed, at order $O(\Delta t^2)$, as follows

$$\partial_t \alpha|^n = \frac{\alpha^{n+1} - \alpha^{n-1}}{2\Delta t}$$
$$\partial_t^2 \alpha|^n = \frac{\alpha^{n+1} - 2\alpha^n + \alpha^{n-1}}{\Delta t^2}$$
$$\partial_t(\alpha \partial_t \alpha)|^n = \frac{\alpha^{n+1}(\alpha^{n+2} - \alpha^n) - \alpha^{n-1}(\alpha^n - \alpha^{n-2})}{4\Delta t^2},$$

(A.1)

where α^n denotes the discrete value of a flow variable $\alpha(t)$ at $t = n\Delta t$ and Δt is the measurement time step. This method properly reconstructs the wave field (see figure A.10), except that the measurement noise induces some spurious oscillations (see green line). This drawback is easily overcome (see blue line in figure A.10) by applying a moving average filter to the pressure measurements. The local method gives similar results than the Fourier one, except at the wave crest where the Fourier method is more accurate.
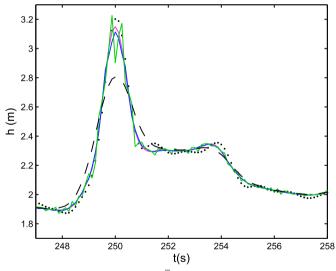

Fig. A.10. Reconstruction of waves observed at La Salie beach (see section 3.3). $\overline{h} = 2.25\,m$, $\delta_m = 0.69$ m. dot: direct acoustic measurement of h; dashed black line: hydrostatic reconstruction ζ_H, Eq. (11); magenta line: $h_{SNL} = \overline{h} + \zeta_{SNL}$, Eq. (13) computed with a Fourier transform; green line: $h_{SNL} = \overline{h} + \zeta_{SNL}$, Eq. (13) computed with the local method (A.14), without measurement noise filtering; blue line: $h_{SNL} = \overline{h} + \zeta_{SNL}$, Eq. (13) computed with the local method (A.14), with a moving average filter of ζ_H over 0.5 s.

References

Abreu, T., Michallet, H., Silva, P.A., Sancho, F., van der, A.,D., Ruessink, B.G., 2013. Bed shear stress under skewed and asymmetric oscillatory flows. Coast. Eng. 73, 1–10.
Berni, C., Michallet, H., Barthélemy, E., 2017. Effects of horizontal pressure gradients on bed destabilization under waves. J. Fluid Mech. 812, 721–751.
Birch, R., Fissel, D.B., Borg, K., Lee, V., English, D., 2004. The capabilities of Doppler current profilers for directional wave measurements in coastal and nearshore waters. In: Oceans'04. MTTS/IEEE Techno-ocean'04, vol. 3, pp. 1418–1427.
Bishop, C.T., Donelan, M.A., 1987. Measuring waves with pressure transducers. Coast. Eng. 11 (4), 309–328.
Bonneton, P., Barthelemy, E., Chazel, F., Cienfuegos, R., Lannes, D., Marche, F., Tissier, M., 2011. Recent advances in Serre-Green Naghdi modelling for wave transformation, breaking and runup processes. Eur. J. Mech. B Fluid 30 (6), 589–597.

Bonneton, P., Lannes, D., 2017. Recovering water wave elevation from pressure measurements. J. Fluid Mech. 833, 399–429.
Cavaleri, L., Ewing, J.A., Smith, N.D., 1978. Measurement of the pressure and velocity field below surface waves. In: Favre, A., Hasselmann, Klaus (Eds.), Turbulent Fluxes through the Sea Surface, Wave Dynamics, and Prediction. Springer US, Boston, MA, pp. 257–272. https://doi.org/10.1007/978-1-4612-9806-9_17.
Dubarbier, B., Castelle, B., Marieu, V., Ruessink, G., 2015. Process-based modeling of cross-shore sandbar behavior. Coast. Eng. 95, 35–50.
Elgar, S., Guza, R.T., 1985. Observations of bispectra of shoaling surface gravity waves. J. Fluid Mech. 161, 425–448.
Elgar, S., Guza, R.T., Raubenheimer, B., Herbers, T.H.C., Gallagher, E.L., 1997. Spectral evolution of shoaling and breaking waves on a barred beach. J. Geophys. Res. 102 (C7), 15797–15805. https://doi.org/10.1029/97JC01010.

Esteva, D., Harris, D., 1970. Comparison of pressure and staff wave gage records. In: Proceedings of the 12th Coastal Engineering Conference, Washington, D.C, pp. 101–116.

Guza, R.T., Thornton, E.B., 1980. Local and shoaled comparisons of sea surface elevations, pressures, and velocities. J. Geophys. Res. 85 (C3), 1524–1530. https://doi.org/10.1029/JC085iC03p01524.

Henderson, S.M., Guza, R.T., Elgar, S., Herbers, T.H.C., Bowen, A.J., 2006. Nonlinear generation and loss of infragravity wave energy. J. Geophys. Res.: Oceans 111 (C12).

Hom-ma, M., Horikawa, K., Komori, S., 1966. Response characteristics of underwater wave gauge. In: Proceedings of the 10th Coastal Engineering Conference, Tokyo, Japan, pp. 99–114.

Lannes, D., 2003. Secular growth estimates for hyperbolic systems. J. Differ. Equ. 190, 466–503.

Lannes, D., Bonneton, P., 2009. Derivation of asymptotic two-dimensional time-dependent equations for surface water wave propagation. Phys. Fluids 21 (1), 016601. https://doi.org/10.1063/1.3053183 (9 pages).

Lannes, D., 2013. The Water Waves Problem: Mathematical Analysis and Asymptotics, Volume 188 of Mathematical Surveys and Monographs. AMS.

Martins, K., Blenkinsopp, C.E., Zang, Z., 2016. Monitoring individual wave characteristics in the inner surf with a 2-dimensional laser scanner (LiDAR). J. Sensors. https://doi.org/10.1155/2016/7965431. Article ID 7965431.

Martins, K., Blenkinsopp, C.E., Almar, R., Zang, Z., 2017. On the influence of swash-based reflection on surf zone hydrodynamics: a wave-by-wave approach. Coast. Eng. 122, 27–43.

Martins, K., Bonneton, P., Frappart, F., Detandt, G., Bonneton, N., Blenkinsopp, C.E., 2017. High frequency field measurements of an undular bore using a 2D LiDAR scanner. Rem. Sens. 9 (5), 462. https://doi.org/10.3390/rs9050462.

Martins, K., Blenkinsopp, C.E., Power, H.E., Bruder, B., Puleo, J.A., Bergsma, E.W.J., 2017. High-resolution monitoring of wave transformation in the surf zone using a LiDAR scanner array. Coast. Eng. 128, 37–43.

Masselink, G., Ruju, A., Conley, D., Turner, I., Ruessink, G., Matias, A., Thompson, C., Castelle, B., Puelo, J., Citerone, V., Wolters, G., 2016. Large-scale Barrier Dynamics Experiment II (BARDEX II): experimental design, instrumentation, test program, and data set. Coast. Eng. 113, 3–18.

Michallet, H., Barthélemy, E., Lammens, A., Marin, G., Vaudelin, G., 2017. Bed motion under waves: plug and sheet flow observations. In: Coastal Dynamics, 2017. Helsingør, Denmark, paper No. 255.

Oliveras, K.L., Vasan, V., Deconinck, B., Henderson, D., 2012. Recovering the water-wave profile from pressure measurements. SIAM J. Appl. Math. 72 (3), 897–918.

Rocha, M.V.L., Michallet, H., Silva, P.A., 2017. Improving the parameterization of wave nonlinearities - the importance of wave steepness, spectral bandwidth and beach slope. Coast. Eng. 121, 77–89.

Senechal, N., Bonneton, P., Dupuis, H., 2002. Field experiment on secondary wave generation on a barred beach and the consequent evolution of energy dissipation on the beach face. Coast. Eng. 46 (3), 233–247.

Shi, F., Kirby, J.T., Harris, J.C., Geiman, J.D., Grilli, S.T., 2012. A high-order adaptive time-stepping TVD solver for Boussinesq modeling of breaking waves and coastal inundation. Ocean Model. 43, 36–51.

Tsai, C.H., Huang, M.C., Young, F.J., Lin, Y.C., Li, H.W., 2005. On the recovery of surface wave by pressure transfer function. Ocean Eng. 32 (10), 1247–1259.

Vasan, V., Oliveras, K., Henderson, D., Deconinck, B., 2017. A method to recover water-wave profiles from pressure measurements. Wave Motion 75, 25–35.

Zijlema, M., Stelling, G., Smit, P., 2011. SWASH: an operational public domain code for simulating wave fields and rapidly varied flows in coastal waters. Coast. Eng. 58 (10), 992–1012.